PHYSICAL REVIEW A **84**, 051404(R) (2011)

XUV ionization of aligned molecules

F. Kelkensberg,[1] A. Rouzée,[1,2] W. Siu,[1] G. Gademann,[1] P. Johnsson,[1,3] M. Lucchini,[4] R. R. Lucchese,[5] and M. J. J. Vrakking[1,2]

[1]*FOM Institute AMOLF, Science Park 104, NL-1098 XG Amsterdam, The Netherlands*

[2]*Max-Born-Institut, Max-Born Strasse 2A, D-12489 Berlin, Germany*

[3]*Department of Physics, Lund University, Post Office Box 118, SE-221 00 Lund, Sweden*

[4]*Department of Physics, Politecnico di Milano, Istituto di Fotonica e Nanotecnologie CNR-IFN, Piazza Leonardo da Vinci 32, 20133 Milano, Italy*

[5]*Department of Chemistry, Texas A&M University, College Station, Texas 77843-3255, USA*

(Received 26 May 2011; published 23 November 2011)

New extreme-ultraviolet (XUV) light sources such as high-order-harmonic generation (HHG) and free-electron lasers (FELs), combined with laser-induced alignment techniques, enable novel methods for making molecular movies based on measuring molecular frame photoelectron angular distributions. Experiments are presented where CO_2 molecules were impulsively aligned using a near-infrared laser and ionized using femtosecond XUV pulses obtained by HHG. Measured electron angular distributions reveal contributions from four orbitals and the onset of the influence of the molecular structure.

DOI: 10.1103/PhysRevA.84.051404 PACS number(s): 33.80.Eh, 42.65.Ky, 82.53.Eb

The making and breaking of chemical bonds typically takes place on a time scale of 100 fs (1 fs $= 10^{-15}$ s) and has motivated the development of femtochemistry experiments, where the time evolution of molecules is commonly probed by exploiting the relation that exists between the structure of a molecule and its photoabsorption spectrum [1]. It follows that the interpretation of these experiments often hinges on a pre-existing understanding of the spectroscopy of the molecule under investigation, and therefore alternative approaches based on the diffraction of electron or light waves are currently actively being researched. In recent years electron diffraction experiments using short electron bunches have already enabled the observation of structural changes in chemical reactions [2], crystals [3], and phase transitions [4]. In these experiments the wavelength of the electrons is small compared to the relevant interatomic distances, inducing diffraction that enables one to resolve structures with sub-nanometer resolution. The creation of electron bunches shorter than 100 fs is a major challenge. Alternatively, one can use diffraction of ultrashort extreme ultraviolet (XUV) or x-ray pulses or the diffraction of electrons that are generated within a molecule through photoionization by an XUV or x-ray pulse. These pulses can be generated by high-order-harmonic generation (HHG) in small-scale laboratories with a duration as short as 80 as [5] and are available with very high fluxes at new FEL facilities that are emerging around the world.

Photoelectrons ejected from a molecule by photoionization contain information on the molecular orbitals from which they are removed. In addition, the outgoing electrons experience the surrounding atoms in the molecule as scattering centers, endowing the photoelectron angular distribution (PAD) with sensitivity to the underlying molecular structure [6]. The extraction of detailed information on orbitals and/or structure is possible provided that the PAD is measured in the molecular frame. This challenge can be met in an elegant way by measuring photoelectrons and fragment ions that are formed from the same parent molecule in coincidence. The requirement of a rapid dissociation accompanied by an axial recoil of the fragment ions can be circumvented by using molecular alignment and orientation techniques [7–9], which allow active control of the angular distribution of a parent molecule before ionization takes place. Photoionization of aligned molecules has previously been explored with UV/near-infrared (IR) radiation [10–12], where it leads to the ejection of photoelectrons with a relatively low kinetic energy. To obtain structural information, the kinetic energy E_k of the ejected electrons must be high enough for the de Broglie wavelength $\lambda_{\text{de Broglie}} = h/\sqrt{2m_e E_k}$ of the electron to be small compared to the interatomic spacings [13]. One proposed solution is ponderomotive acceleration and subsequent recollision of tunnel-ionized photoelectrons using an intense, low-frequency laser field, as demonstrated in N_2, O_2 [14] and Xe [15]. An alternative method is to measure high-energy photoelectrons that are ejected in single-photon ionization by XUV or x-ray light. This is the approach followed in the current paper, where we present results for the ionization of aligned CO_2 molecules using femtosecond XUV pulses from a HHG source.

XUV pulses extending from harmonic H11 (17.5 eV) to H31 (49.3 eV) were generated by HHG in argon, using approximately 1-mJ, 780-nm, 30-fs full-width at half-maximum (FWHM) laser pulses from a Ti:Sa amplifier. In Fig. 1(a), an experimental photoelectron momentum distribution is shown that was measured for ionization of randomly oriented CO_2 molecules by the XUV pulse, making use of a velocity map imaging spectrometer [16]. From this momentum distribution, photoelectron kinetic energy spectra were extracted by integrating over an acceptance angle of $\pm 20^\circ$ parallel ($\theta_{e^-} = 0^\circ$) and perpendicular ($\theta_{e^-} = 90^\circ$) to the laser polarization axis [see Fig. 1(b)]. The spectra contain a series of peaks, since each harmonic order can produce several ionic states that differ in their ionization potential (I_p). Contributions from four ionization channels can be recognized, corresponding to ionization from the highest occupied molecular orbital (HOMO) ($X\,^2\Pi_g$, $I_p = 13.8$ eV), the HOMO-1 ($A\,^2\Pi_u$, $I_p = 17.6$ eV), the HOMO-2 ($B\,^2\Sigma_u^+$, $I_p = 18.1$ eV), and the HOMO-3 ($C\,^2\Sigma_g^+$, $I_p = 19.4$ eV) orbitals. The resolution of the spectrometer ($\Delta E/E = 2\%$)

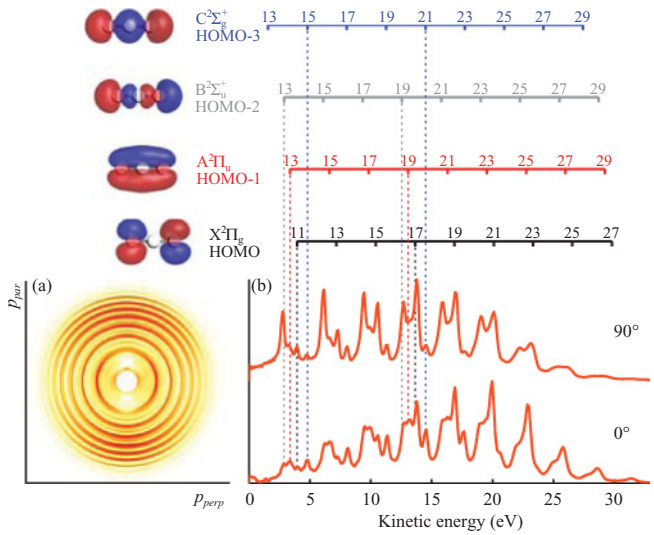

FIG. 1. (Color online) (a) Photoelectron momentum distribution for photoionization of randomly oriented CO_2 molecules by an XUV pulse generated by means of HHG and (b) photoelectron spectra for electrons emitted parallel ($\theta_{e^-} = 0°$) and perpendicular ($\theta_{e^-} = 90°$) to the polarization of the ionizing XUV pulse, obtained by integrating over a finite acceptance angle of $\pm 20°$. The peaks in the spectra in panel (b) are the result of the presence of four ionization channels corresponding to the HOMO ($X\,^2\Pi_g$, $I_p = 13.8$ eV), the HOMO-1 ($A\,^2\Pi_u$, $I_p = 17.6$ eV), the HOMO-2 ($B\,^2\Sigma_u^+$, $I_p = 18.1$ eV), and the HOMO-3 ($C\,^2\Sigma_g^+$, $I_p = 19.4$ eV) orbitals of CO_2. Each channel can be accessed by multiple harmonic orders in the XUV pulse, which are indicated in the top part of the figure.

allowed one to resolve peaks in the photoelectron spectra (PES) from the different ionization channels up to electron energies of about 15 eV. The PAD $P(E_k, \cos\theta_{e^-})$ can be decomposed as follows: $P(E_k, \cos\theta_{e^-}) = \sigma(E_k)[1 + \beta_2(E_k)P_2(\cos\theta_{e^-}) + \beta_4(E_k)P_4(\cos\theta_{e^-}) + \cdots]$, where $\sigma(E_k)$ is the photoionization cross section and $P_l(\cos\theta_{e^-})$ the lth-order Legendre polynomial. For single-photon ionization of an isotropic sample, only the β_2 parameter is nonzero. When the β_2 parameter is positive (negative), the electron emission predominantly occurs parallel (perpendicular) to the laser polarization. In Fig. 1, the angular distribution of the HOMO-1 and HOMO-3 peaks parallel to the laser polarization (positive β_2 parameter), whereas electrons from the HOMO and HOMO-2 orbitals are ejected predominantly perpendicular to the laser polarization (negative β_2 parameter).

Field-free molecular alignment was achieved by exposing the CO_2 molecules to a moderately strong (5–15 TW/cm^2), 780-nm, 300-fs FWHM laser pulse [7]. This led to alignment and antialignment ("planar delocalization") at regular time intervals, as observed using a measurement of the angular distribution of O^+ ions resulting from Coulomb explosion by the XUV pulse [17]. Figure 2(a) shows the alignment $\langle\cos^2\theta_{O^+}\rangle$ of the O^+ ions as a function of the delay between the XUV pulse and the alignment pulse. The measurement is shown around the second revival of the molecular alignment ($t \approx 21$ ps), where the molecules first become aligned (high value of $\langle\cos^2\theta_{O^+}\rangle$) and subsequently antialigned (low value of $\langle\cos^2\theta_{O^+}\rangle$). Significant changes in the photoelectron momentum distributions around this revival are revealed in Figs. 2(b) and 2(c), where the evolution of the yield [Fig. 2(b)] and the β_2 parameter [Fig. 2(c)] of the photoelectrons are shown for the four aforementioned orbitals for a selected set of harmonics. The different ionization channels show distinct behavior in both the yield and the β_2 parameter. The yield of electrons from the HOMO and HOMO-1 orbitals is suppressed (enhanced) when the molecules are aligned (antialigned), whereas the yields of photoelectrons corresponding to the HOMO-2 and HOMO-3 orbitals show the opposite behavior. The β_2 parameter of the HOMO channel is only slightly affected by the alignment of the molecules, whereas the HOMO-1 and HOMO-2 angular distributions become less (more) peaked along the laser polarization for alignment (antialignment), with the opposite being true for the HOMO-3 channel. The enhancement or suppression of the photoionization yield for (anti)aligned molecules that is observed for a given orbital directly relates to the parallel or perpendicular character of the transition from the ground state of the molecule to the final state of the molecular ion + photoelectron. The final state can have either Σ_u or Π_u total symmetry, which results in parallel and perpendicular transitions, respectively [18]. The yield of ionic states that are formed by a parallel (perpendicular) transition increases (decreases) upon alignment of the molecule.

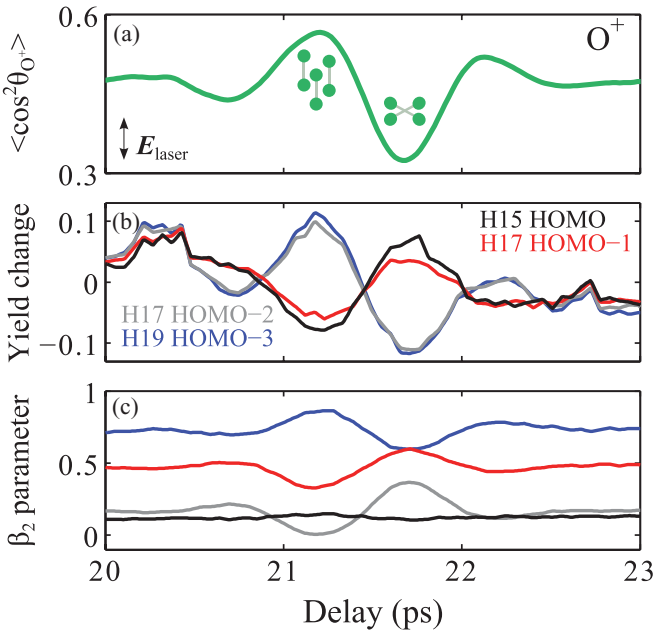

FIG. 2. (Color online) (a) $\langle\cos^2\theta_{O^+}\rangle$ of O^+ fragments as a function of the delay between the IR and XUV pulses around the second alignment revival. Channel-specific evolution of the (b) yield and (c) β_2 parameter of the PAD around this revival.

To analyze the experimental results, PADs from photoionization of aligned CO_2 molecules were calculated by an electron-molecule quantum scattering method that has previously been successfully applied to calculate molecular-frame PADs (MFPADs) recorded with synchrotron radiation [19,20]. The method is based on the multichannel Schwinger configuration interaction method (MCSCI), where the initial and final ionic states are represented as configuration interaction (CI) wave functions. All calculations were done at the experimental equilibrium geometry with R(C-O) = 1.1621 Å,

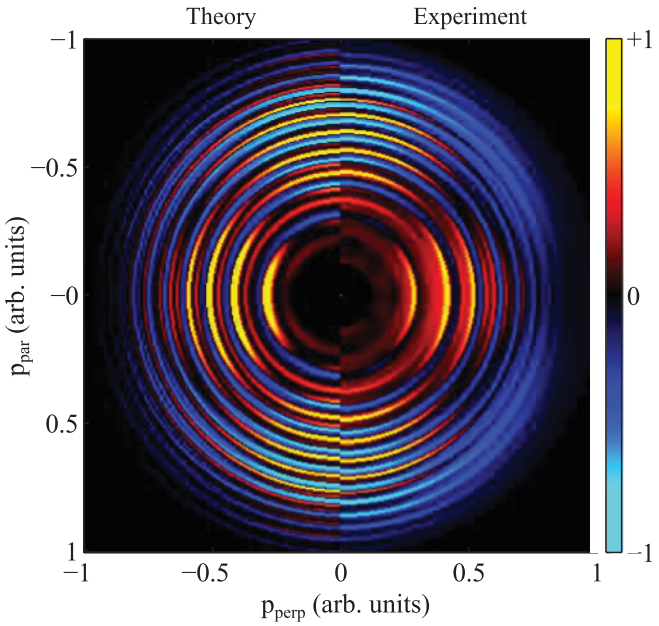

FIG. 3. (Color online) Comparison between an experimentally measured (left) and a theoretically calculated (right) differential photoelectron momentum distribution, representing the difference between two momentum distributions that are obtained at maximum alignment and at planar delocalization.

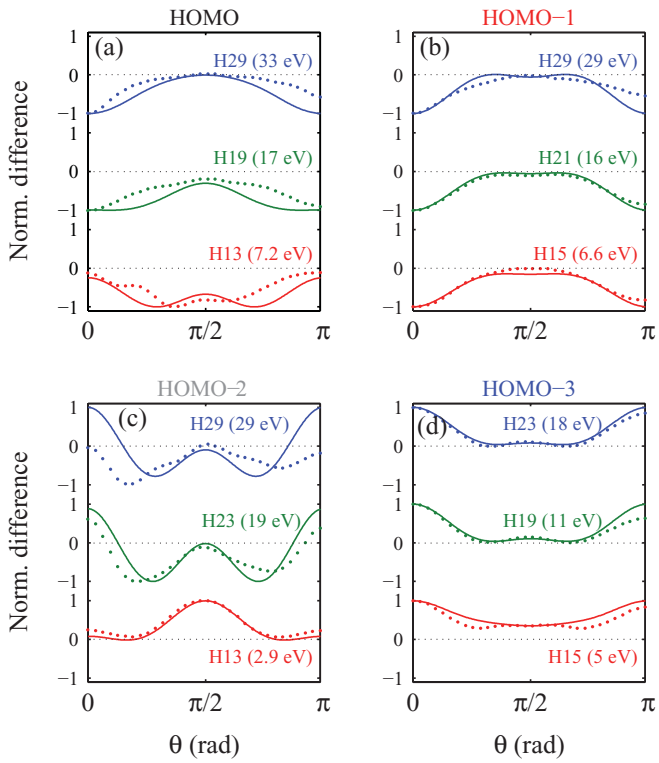

FIG. 4. (Color online) Comparison between the experimentally measured (dotted lines) and calculated (solid lines) differential PADs for ionizing of (a) the HOMO, (b) the HOMO-1, (c) the HOMO-2, and (d) the HOMO-3. The photoelectron kinetic energy is shown in brackets.

and the four outer valence ion states of CO_2^+ that were found to contribute to the experimental data ($X\,^2\Pi_g$, $A\,^2\Pi_u$, $B\,^2\Sigma_u^+$, $C\,^2\Sigma_g^+$) were included. To simulate the PADs from aligned and antialigned CO_2 molecules, the experimental alignment distributions following from the O^+ angular distribution data were used. Differential cross sections $\sigma_i^\alpha(E_{\mathrm{XUV}},\theta_{e^-})$ were calculated as a function of the photon energy E_{XUV} and angle of emission θ_{e^-} for each ionization channel i and for each alignment distribution α. Using $\sigma_i^\alpha(E_{\mathrm{XUV}},\theta_{e^-})$, the experimental PADs were constructed using a fitting procedure for the intensity and the width of the individual harmonics. Differential PADs were obtained by taking the difference between the PAD at maximum alignment and antialignment.

Figures 3 and 4 shows a comparison between the experimentally measured and calculated differential PADs. Figure 3 shows a comparison between experimentally measured (left) and theoretically calculated (right) differential photoelectron momentum maps. Positive (red and yellow) and negative (blue) contributions occur, depending on the symmetry (parallel or perpendicular) of the transition under consideration. The comparison is further elaborated in Figs. 4(a)–4(d), where experimental (dotted lines) and calculated (solid lines) differential PADs are plotted for all four channels for a selected set of harmonics. The negative contributions observed for the HOMO [Fig. 4(a)] and HOMO-1 [Fig. 4(b)] indicate an enhancement in the photoelectron yield when the molecules are aligned perpendicularly to the laser polarization axis and indicate a predominantly perpendicular transition to the final state, i.e., a Π_u total symmetry. Positive values for the HOMO-3 [Fig. 4(d)] reveal that the ionization of this orbital occurs predominantly via a parallel transition, where the final-state symmetry is given by Σ_u. The differential PAD corresponding to the HOMO-2 [Fig. 4(c)] dramatically changes around a photoelectron kinetic energy of 15 eV. At low energies only positive values are observed, whereas at higher energies negatives values emerge. This shows that the symmetry of the final state changes from Σ_u to Π_u, which necessarily is accompanied by a change in the symmetry of the outgoing electron.

The differential PADs of all channels evolve with the photoelectron kinetic energy. The differential PAD for the HOMO [Fig. 4(a)] shows dips for low kinetic energies (7.2 eV) centered at $\theta_{e^-} = 45°$, which move to $\theta_{e^-} = 0°$ and $\theta_{e^-} = 180°$ (i.e., along the laser polarization) at high kinetic energy. In the case of the HOMO-2 orbital [Fig. 4(c)], the differential PAD shows a pronounced maximum perpendicular to the laser polarization axis ($\theta_{e^-} = 90°$) at low kinetic energy. At higher energies, maxima also appear along the laser polarization axis, leaving a minimum at $\theta_{e^-} = 45°$. Ionization from the HOMO-3 orbital [Fig. 4(d)] leads to positive values in the differential PAD at all angles for low energies, while at higher energies dips develop at $\theta_{e^-} = 45°$. Previously, the energy dependence of MFPADs was observed in K-shell photo-ionization of CO and N_2 [6,21] and was related to the occurrence of shape resonances. In CO_2, a σ^* resonance in the photoionization of the HOMO-3 orbital at a photon energy of 32 eV could influence the PADs [18]. This is at variance, however, with the observation that the suppression of interchannel couplings in the calculation revealed no significant differences. Therefore,

the evolution of the angular distribution of the ejected photoelectron may be seen as a manifestation of the influence of the molecule structure on the MFPAD, where the influence of the Coulomb field of the molecule on the trajectories of the outgoing electrons is strongly dependent on kinetic energy. In this way information on the structure of the molecule finds its way in the photoelectron angular distribution. As such, both these experimental results and the demonstration that PADs for photoionization of aligned molecules can successfully be modeled pave the way toward experiments where structural and electronic dynamics during photochemical reactions are recorded by measuring the evolution of PADs for aligned, time-evolving molecular systems. Indeed, a natural extension of this work will be to add a third pulse that initiates a photochemical reaction in the aligned molecule, such as its dissociation or isomerization. Experiments of this kind are likely to be vigorously pursued at emerging XUV and x-ray FELs such as Free electron LASer of Hamburg, Linac Coherent Light Source of Stanford, Spring-8, and the European X-ray Free Electron Laser. By using HHG sources it may even be possible to extend these methods to the investigation of dynamics on the few-femtosecond or few-attosecond time scales.

This work is part of the research program of the Stichting voor Fundamenteel Onderzoek der Materie (FOM), which is financially supported by the Nederlandse organisatie voor Wetenschappelijk Onderzoek (NWO). P. J. acknowledges the support of the Swedish Research Council. R.R.L. acknowledges support from the Chemical Sciences, Geosciences, and Biosciences Division, Office of Basic Energy Sciences, Office of Science, US Department of Energy, and from the Robert A. Welch Foundation of Houston, Texas, under Grant No. A-1020.

[1] A. H. Zewail, Angew. Chem. Int. Ed. Engl. **39**, 2586 (2000).
[2] H. Ihee, V. A. Lobastov, U. M. Gomez, B. M. Goodson, R. Srinivasan, C. Y. Ruan, and A. H. Zewail, Science **291**, 458 (2001).
[3] B. J. Siwick, J. R. Dwyer, R. E. Jordan, and R. J. D. Miller, Science **302**, 1382 (2003).
[4] N. Gedik, D. S. Yang, G. Logvenov, I. Bozovic, and A. H. Zewail, Science **316**, 425 (2007).
[5] E. Goulielmakis *et al.*, Science **320**, 1614 (2008).
[6] A. Landers *et al.*, Phys. Rev. Lett. **87**, 013002 (2001).
[7] F. Rosca-Pruna and M. J. J. Vrakking, Phys. Rev. Lett. **87**, 153902 (2001).
[8] O. Ghafur, A. Rouzee, A. Gijsbertsen, W. K. Siu, S. Stolte, and M. J. J. Vrakking, Nat. Phys. **5**, 289 (2009).
[9] H. Stapelfeldt and T. Seideman, Rev. Mod. Phys. **75**, 543 (2003).
[10] M. Tsubouchi, B. J. Whitaker, L. Wang, H. Kohguchi, and T. Suzuki, Phys. Rev. Lett. **86**, 4500 (2001).
[11] C. Z. Bisgaard, O. J. Clarkin, G. R. Wu, A. M. D. Lee, O. Gessner, C. C. Hayden, and A. Stolow, Science **323**, 1464 (2009).
[12] Y. Tang, Y. I. Suzuki, T. Horio, and T. Suzuki, Phys. Rev. Lett. **104**, 073002 (2010).
[13] F. Krasniqi, B. Najjari, L. Struder, D. Rolles, A. Voitkiv, and J. Ullrich, Phys. Rev. A **81**, 033411 (2010).
[14] M. Meckel *et al.*, Science **320**, 1478 (2008).
[15] Y. Huismans *et al.*, Science **331**, 61 (2011).
[16] A. T. J. B. Eppink and D. H. Parker, Rev. Sci. Instrum. **68**, 3477 (1997).
[17] F. Lepine *et al.*, J. Mod. Opt. **54**, 953 (2007).
[18] I. Cacelli, R. Moccia, and R. Montuoro, Phys. Rev. A **63**, 012512 (2000).
[19] R. R. Lucchese, K. Takatsuka, and V. McKoy, Phys. Rep. **131**, 147 (1986).
[20] R. R. Lucchese, A. Lafosse, J. C. Brenot, P. M. Guyon, J. C. Houver, M. Lebech, G. Raseev, and D. Dowek, Phys. Rev. A **65**, 020702 (2002).
[21] R. Guillemin *et al.*, Phys. Rev. Lett. **89**, 033002 (2002).